ACS APPLIED NANO MATERIALS

www.acsanm.org Article

Graphene/WS_2 Nanodisk Van der Waals Heterostructures on Plasmonic Ag Nanoparticle-Embedded Silica Metafilms for High-Performance Photodetectors

Mohammed Alamri,* Bo Liu, Seyed M. Sadeghi, Dan Ewing, Amy Wilson, Jennifer L. Doolin, Cindy L. Berrie, and Judy Wu*

Cite This: *ACS Appl. Nano Mater.* 2020, 3, 7858−7868 Read Online

ACCESS | Metrics & More | Article Recommendations | Supporting Information

ABSTRACT: Coupling plasmons and excitons provide a promising approach to enhance the performance of photodetectors based on two-dimensional (2D) atomic layer heterostructures. Herein, we report a nanohybrid photodetector achieved by transferring a nonmetallic plasmonic WS_2 nanodisk/graphene van der Waal (vdW) heterostructure grown using chemical vapor deposition, on metallic plasmonic Ag nanoparticles embedded in 20 nm thick silica (AgNP-metafilm) fabricated using in situ Ag and Si evaporation through a shadow mask. This nanohybrid photodetector enables not only superposition of the plasmonic effects from the two plasmonic nanostructures, but also the effective coupling of the plasmons and excitons in WS_2 nanodisks upon illumination. This leads to a high responsivity of 11.7 A/W on the graphene/WS_2 nanodisks/AgNP-metafilm under an incident illumination power of 5.5×10^{-8} W at 450 nm, which represents a 500% enhancement over that of the counterpart without the AgNP-metafilm. The finite element time-domain simulation of the local light field distribution indicates that the enhancement can be attributed to enhancement of exciton (electron−hole pair) excitation and exciton−plasmon coupling in the graphene/WS_2 nanodisks/AgNP-metafilm photodetectors. In addition, the approach for fabrication of the graphene/WS_2 nanodisks/AgNP-metafilm heterostructures is scalable and cost efficient and hence promising for commercial applications.

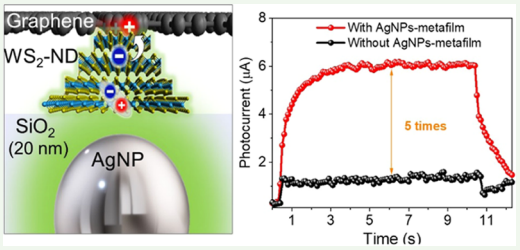

KEYWORDS: *Ag nanoparticle-metafilm, WS_2 nanodisk, graphene, photodetector, optoelectronics*

1. INTRODUCTION

Two-dimensional (2D) atomic materials such as graphene and transition-metal dichalcogenides (TMDCs) have received much attention due to their superior optical and electronic properties. The combination of graphene and TMDCs in the so-called TMDC/graphene van der Waals (vdW) heterostructure nanohybrids can take advantage of graphene's high charge carrier mobility[1] and broadband, low optical absorption (~2.3% for single-layer graphene)[2] with TMDCs' strong light absorption tunable by their band gaps,[3,4] providing an excellent scheme for the design of high-performance optoelectronic devices. In these TMDC/graphene or more generally semiconductor sensitizer/graphene nanohybrids,[5−10] light is absorbed by the semiconductor photosensitizer (such as TMDCs), generating excitons or electron−hole pairs in the sensitizer. The built-in electric field at the sensitizer/graphene interface assists both exciton dissociation to free charge carriers and charge transfer from the sensitizer to graphene. The high mobility of the charge carriers in graphene leads to a very short transit time, $\tau_{transit}$, of the transferred carriers (one type depending on the built-in field at the sensitizer/graphene interface) between the two electrodes on graphene, while the other type of charge carriers remain trapped in the sensitizer during the exciton lifetime ($\tau_{lifetime}$). The exciton lifetime regards the time scale the electron−hole recombination occurs. The holes would be trapped in the WS_2-NDs after the electrons transfer to graphene within the exciton lifetime before the electron−hole recombination. It should be pointed out that graphene may not be a good choice as active optical materials since it does not have a band gap. However, graphene can provide an excellent transport pathway for photoexcited carriers due to its high mobility. Therefore, a nanohybrid structure of the graphene and semiconductor material combines the advantage of the semiconductor sensitizer to absorb the incident light and graphene acts as an efficient channel to transport the photoexcited carriers. Since photoconductive gain (G) in the sensitizer/graphene nanohybrids is proportional to the ratio of the $\tau_{lifetime}$ to the $\tau_{transit}$, G up to 10^8−10^{10} in the semiconductor quantum dot/graphene

Received: May 18, 2020
Accepted: August 3, 2020
Published: August 10, 2020

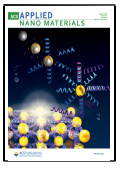

https://dx.doi.org/10.1021/acsanm.0c01360
ACS Appl. Nano Mater. 2020, 3, 7858−7868

nanohybrid photodetectors through a combination of the strong quantum confinement in the quantum dots (QDs) and high carrier mobility in graphene has been achieved.[4−10] Consequently, a significant improvement in photoresponse has been reported in the QD/graphene and TMDC/graphene nanohybrids.[6,7,11] Konstantatos et al. reported the first PbS QD/graphene nanohybrid photodetector.[5] A high gain of ~10^8 and a photoresponsivity of ~10^7 A/W in the visible spectrum were demonstrated. Comparable photoconductive gains and high photoresponsivity have also been reported in other nanohybrids.[6,8,9] For example, a ZnO QD/graphene nanohybrid photodetector was reported to exhibit a high ultraviolet photoresponsivity of >10^8 A/W due to the high gain exceeding 10^9.[6,8] On the MoS_2 (few-layer)/transfer-free graphene nanohybrid photodetectors, a high responsivity of 835 mA/W was reported in the visible spectrum.[11] Kuiri et al. reported a responsivity of 20 mA/W on an infrared photodetector based on $MoTe_2$/graphene heterostructures nanohybrids.[7] A clean interface is required between the semiconductor sensitizer and graphene for charge transfer and to establish a native electric field due to the electronic band edge alignment across the interface. Defects and impurities at the interface, which can occur especially at the vdW interface formed through mechanical stacking of the semiconductor sensitizer/graphene heterostructures, can significantly degrade the photodetector performance resulting in low and slow photoresponse. Indeed, transfer-free or postannealed TMDC/graphene vdW heterostructure nanohybrids have exhibited fast and high photoresponse due to the significant reduction of interfacial defects.[10−12]

One of the fundamental issues limiting further enhancement of the performance of the TMDC/graphene and QDs/graphene nanohybrid photodetectors is the limited light absorption due to the small thickness of the sensitizer (sub-nm for the monolayer TMDCs, few nm in the few-layer TMDCs or single-layer QDs). To address this issue, various approaches have been explored. One promising approach is implementation of plasmonic metallic nanostructures for light trapping in the vicinity of the metal surface[13−16] to enhance light absorption in the semiconductor sensitizer in close proximity. For example, the photoresponsivity of graphene was enhanced by about 400% by transferring the prefabricated Au nanoparticles (AuNPs) on graphene.[16] In addition, J. Miao et al. demonstrated a 3-fold enhancement of the photoresponse after AuNPs were deposited onto few-layer MoS_2 phototransistors.[15] A similar light-trapping benefit on the sensitivity of Raman spectroscopy was also reported through surface-enhanced Raman spectroscopy (SERS) via implementation of the plasmonic metal nanostructures on graphene,[17,18] MoS_2,[19] and MoS_2/graphene heterostructures.[20] Another approach is to generate localized surface plasmonic resonance (LSPR) effects directly in the nanostructured semiconductor sensitizers via carrier doping[21] thereby enhancing their light absorption. For example, in $Fe_{1-x}S_2$ QD/graphene nanohybrid photodetectors, a strong LSPR effect was induced in the $Fe_{1-x}S_2$ QDs via carrier doping, resulting in significantly enhanced light absorption in plasmonic $Fe_{1-x}S_2$ QDs and thereby enhancing responsivity in the $Fe_{1-x}S_2$ QDs/graphene photodetectors.[22−24] Similarly, LSPR can be induced in the TMDC nanodisks (NDs) in the TMDC-NDs/graphene nanohybrids. Interestingly, SERS sensitivity considerably higher than that of the AuNP/graphene SERS substrates was achieved on TMDC-NDs/graphene.[25] In the TMDC-ND/graphene nanohybrid photodetectors, a seven-fold enhancement in the photoresponsivity was achieved with respect to the counterpart with a TMDC continuous layer sensitizer.[10] These results illustrate that coupling plasmons and excitons can provide an effective scheme to enhance the light absorption of the thin sensitizers in the sensitizer/graphene nanohybrids using either metallic plasmonic nanostructures or LSPR in the semiconductor nanostructure sensitizers. A question arises as to whether these two approaches could be combined to yield further enhanced light absorption and device performance of the TMDC/graphene nanohybrid photodetectors.

In this work, we explore integration of the two approaches. Specifically, a graphene/WS_2-ND heterostructure was transferred on a AgNP-metafilm consisting of a layer of AgNPs embedded in a 20 nm thick SiO_2 overlayer,[26] aiming to further enhance the optical absorption and hence the photoresponse of the graphene/WS_2-ND/AgNP-metafilm photodetector. A key step is the development of a new process to obtain the transferrable graphene/WS_2-ND heterostructures, which has resolved the issue of the AgNP-metafilm degradation during the WS_2-ND growth through exposure to sulfur vapor at elevated temperatures. The obtained transferrable graphene/WS_2-NDs heterostructures are intact with comparable optoelectronic performance to their counterpart obtained through layer-by-layer growth of WS_2-NDs on graphene using chemical vapor deposition (CVD). This process was further developed to transfer the graphene/WS_2-NDs on a variety of substrates including SiO_2/Si with prefabricated Au electrodes and the AgNP-metafilm located in the channel between the electrodes. In the obtained graphene/WS_2-ND/AgNP-metafilm nanohybrid photodetectors, the strong plasmon−exciton coupling is illustrated through broadband enhancement of light absorption and photoresponsivity in the spectral range of 400−700 nm, with a maximum 5-fold enhancement in the photoresponsivity at the LSPR frequency (~442 nm) of the AgNP-metafilm compared with reference devices of the graphene/WS_2-NDs without the AgNP-metafilm. In the following, we report our results.

2. EXPERIMENTAL AND SIMULATION

2.1. CVD Graphene Synthesis. The synthesis of graphene was carried out in a quartz tube reactor (25 mm inner diameter) inside a CVD system. The details of the CVD graphene synthesis process have been reported previously.[27,28] Briefly, a 25 μm thick Cu foil strip was inserted into the center of the quartz tubular reactor. H_2 gas (40 sccm) was introduced into the CVD system while increasing the sample temperature to 1050 °C for graphene growth. After 1 h of annealing of the Cu foil at 1050 °C, H_2 was reduced to 7 sccm and CH_4 (40 sccm) was introduced to initiate the graphene growth for 30 min. After the graphene growth was completed, the CVD heater for the sample was turned off and the sample was naturally cooled to room temperature under the protection of the flowing H_2.

2.3. WS_2-ND Growth. WS_2-NDs were grown on SiO_2/Si substrates. A $(NH_4)_2WS_4$ precursor solution with a concentration of 0.1 wt % was prepared by dissolving (10 mg) ammonium tetrathiotungstate ($(NH_4)_2WS_4$) powder in 10 mL of *N*,*N* dimethylformamide (DMF) and was sonicated for 30 min at room temperature. A precleaned SiO_2/Si substrate with a 500 nm SiO_2 thickness was immersed into the $(NH_4)_2WS_4$ precursor solution. The dip-coated SiO_2/Si substrate was then placed on a spin coater and spun at 3000 rpm for 60 s to obtain a uniform, ultrathin layer of the $(NH_4)_2WS_4$ precursor over the entire substrate. Afterward, the sample was placed in a quartz tube CVD furnace and heated to 450 °C under the flowing carrier gas of mixed Ar (40 sccm) and H_2 (10 sccm) for 1 h. The sulfur powder positioned upstream was used to generate a

https://dx.doi.org/10.1021/acsanm.0c01360
ACS Appl. Nano Mater. 2020, 3, 7858−7868

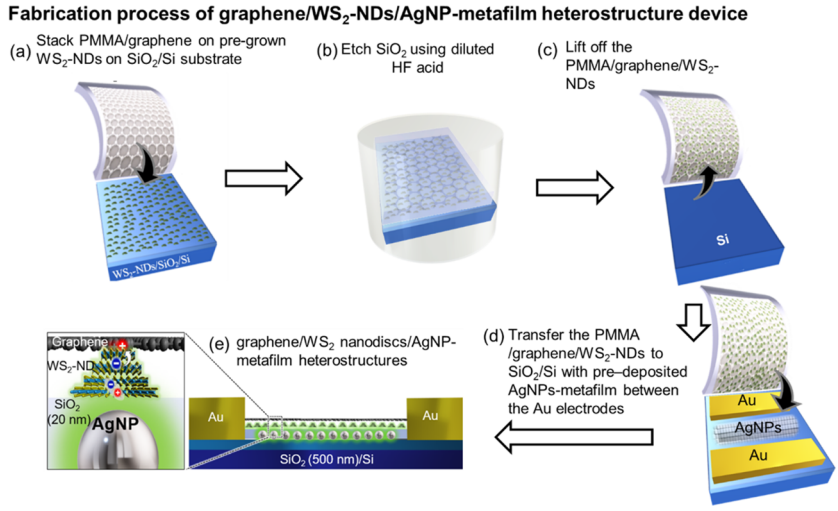

Figure 1. Schematic illustration of the graphene/WS_2-ND/AgNP-metafilm heterostructure device fabrication process: (a) stacking PMMA/graphene on pregrown WS_2-NDs on the SiO_2/Si substrate; (b) etching SiO_2 using diluted HF acid; (c) lift off the PMMA/graphene/WS_2-NDs; (d) transferring the PMMA/graphene/WS_2-NDs to SiO_2/Si with the predeposited AgNP-metafilm between the Au electrodes; and (e) completing the graphene/WS_2-ND/AgNP-metafilm heterostructure device after the removal of PMMA. The inset shows a zoom-in view of the device cross section with a WS_2-ND on top of the 20 nm thick SiO_2 spacer over a AgNP.

sulfur vapor that was carried to the sample by the carrier gas for reaction to form the WS_2-NDs. The pressure was maintained at ~50 mTorr during the WS_2-ND growth. After the growth, the WS_2-ND/SiO_2/Si sample was cooled down naturally to room temperature by turning off the power of the CVD system.

2.4. Fabrication of Transferrable Graphene/WS_2-NDs. To fabricate graphene/WS_2-ND samples that can be transferred on to other surfaces such as the AgNP-metafilms, a new process was developed in this work that takes two major steps. In the first step, a thoroughly cleaned CVD graphene with the supporting poly(methyl methacrylate) (PMMA) layer after removal of the Cu foil[28,29] was placed on top of a WS_2-NDs/SiO_2/Si sample with graphene in contact with the WS_2-NDs. The entire sample assembly was then heated on a hot plate at 80 °C for 1 h to enhance the adhesion of graphene to the WS_2-NDs. In the second step, the entire sample assembly was soaked in diluted (45−48%) hydrofluoric acid (HF) in DI water for 5 min at room temperature to etch the SiO_2 (500 nm in thickness) on the SiO_2/Si substrates. The PMMA/graphene/WS_2-NDs released from the SiO_2/Si substrates were cleaned thoroughly with DI water and were ready for transfer. This sample is different from the WS_2-ND/graphene photodetector with the WS_2-NDs being directly grown on the graphene/SiO_2/Si without transfer since the latter would have a cleaner interface with minimal residues left in the wet transfer progress.[10]

2.5. AgNP-Metafilm and Au/Ti Electrode Fabrication. The source and drain electrodes of Au/Ti (40/10 nm) for the photodetectors were deposited on the SiO_2/Si substrates using electron-beam evaporation through a metal shadow mask. The separation between the two electrodes (or the channel length) is about 250 μm. The AgNP-metafilm was in situ fabricated using electron-beam evaporation of Ag of a nominal thickness of 8 nm at an elevated temperature of ~300 °C under high vacuum (~10^{-6} Torr or better) for 30 min to obtain AgNPs through in situ self-organization[26,30] followed with an in situ evaporation of a SiO_2 layer with a thickness of 20 nm to form the AgNP-metafilm. To prevent formation of electrical shorts between the AgNPs and the Au/Ti electrodes, the AgNP-metafilm was deposited within the channel area with a 200 μm spacing to the Au/Ti source and drain electrodes using a shadow mask.

2.6. Graphene/WS_2-ND/AgNP-Metafilm Photodetector Fabrication and Characterization. The graphene/WS_2-NDs were placed face-down (with the WS_2-NDs toward the AgNP-metafilm) on the SiO_2/Si substrates with prefabricated Au electrodes and AgNP-metafilm. PMMA was then removed using acetone to complete the fabrication of the graphene/WS_2-NDs/AgNP-metafilm photodetectors. This robust method, especially the process for fabrication of the transferrable graphene/WS_2-NDs, is unique and advantageous in terms of preventing degradation of the LSPR effect of the AgNPs due to the exposure to sulfur vapor used for WS_2-ND growth. In fact, significant degradation of the LSPR effect of the AgNPs (without the SiO_2 overlayer) and AgNP-metafilms (with the 20 nm thick SiO_2 overlayer) has been confirmed in our experiment as we shall discuss in detail later. In this study, we have found that a 20 nm thick SiO_2 layer can effectively and uniformly block the electrical current leakage between the graphene/WS_2-NDs and the AgNP-metafilm. Based on the FDTD simulation, the evanescent field in the AgNP-metafilm could extend tens of nm to reach the graphene/WS_2-ND layer even with the addition of the SiO_2 coating. It should be pointed out that replacing the evaporated SiO_2 layer (typically defective) with a less defective dielectric may allow an even smaller distance between the AgNP-metafilm and graphene/WS_2-ND photodetector and hence stronger coupling between the plasmons and excitons from the AgNPs and WS_2-NDs, respectively. Optical images of the samples were taken using a Nikon Eclipse LV 150 optical microscope with a CCD camera. Raman spectra and Raman maps of graphene and WS_2-NDs were collected using a Witec Alpha300 Confocal Raman microscope. Atomic force microscope (AFM, Witec Alpha300) was used to analyze the vertical and lateral dimensions of the WS_2-NDs. AFM images of the SiO_2/AgNP films were collected in contact mode at a scan rate of approximately 1.0 Hz using a Multimode AFM with a Nanoscope IIIA controller from Digital Instruments. Standard silicon nitride probe tips (Bruker, NP-S, k ~ 0.06 N/m) were used for imaging. All images were collected with the same probe tip. Three different representative regions between the two electrodes were imaged at scan sizes of 10 × 10, 2.0 × 2.0, and 1.0 × 1.0 μm^2. Average surface roughness (R_a) was measured using the Nanoscope software in the AFM for each of the scans. In addition, the images were collected for a sample without the SiO_2 coating over the Ag nanoparticles. Scanning electron microscopy (SEM) images were taken using a JEOL JSM-6380 scanning electron microscope to characterize the morphology of the AgNP-metafilm including the shape and size of the AgNPs. The current−voltage (I−V) characteristics of the photodetectors were measured using a CHI660D electrochemical workstation. An Oriel Apex monochromatic illumi-

https://dx.doi.org/10.1021/acsanm.0c01360
ACS Appl. Nano Mater. 2020, 3, 7858−7868

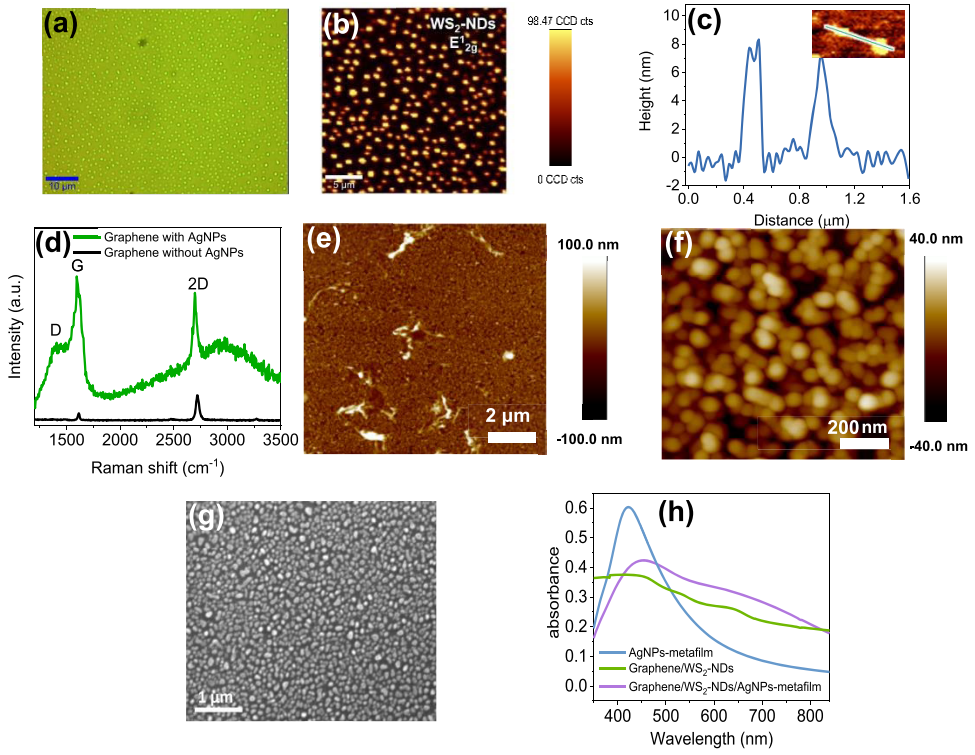

Figure 2. (a) Optical and (b) Raman image of WS_2-NDs. (c) Height profile of WS_2-NDs. Inset: AFM image of WS_2-NDs. (d) Raman spectra of graphene on SiO_2/Si (black) and graphene on SiO_2/Si with AgNPs (green). Representative contact mode AFM images of SiO_2(20 nm)/AgNPs: (e) 10 × 10 μm^2 area, (f) 1.0 × 1.0 μm^2 image of zoomed-in area within (e). (g) SEM image of the AgNPs. (h) UV−vis absorption spectra of AgNP-metafilm (blue), graphene/WS_2-NDs (green), and graphene/WS_2-ND/AgNP-metafilm (purple).

nator was used to measure the temporal photoresponse at selected wavelengths. To measure the optical absorption spectra, the graphene/WS_2-ND heterostructures were transferred onto the transparent fused silica substrates with and without the prefabricated AgNP-metafilm on the substrates. An ultraviolet/visible spectrophotometer (Perkin Elmer, LAMBDA 35) was used to collect the optical absorption spectra in the visible range for the samples used in this work.

2.7. Finite Difference Time-Domain (FDTD) Simulation. To study plasmonic mode profiles of the AgNPs and their impact on the device performance, the Lumerical Finite Difference Time-Domain (FDTD) solutions software (2020a Finite Different IDE) was deployed to calculate the electromagnetic field distribution around a AgNP in the graphene/WS_2-ND/AgNP-metafilm nanohybrid. Specifically, the Device Mutliphysics Simulation Suite of this software was used by setting up different components to replicate the system of the graphene/WS_2-NDs on the AgNP-metafilm as closely as possible. The mesh sizes were varied between 1 and 0.5 nm to accommodate different sizes of the AgNPs. The source configuration was set up such that light reached the layer representing the graphene/WS_2-NDs first and then the AgNP-metafilm.

3. RESULTS AND DISCUSSION

Figure 1 illustrates schematically the device fabrication process developed in this work to generate transferrable graphene/WS_2-NDs that can be transferred on the AgNP-metafilm for the high-performance graphene/WS_2-ND/AgNP-metafilm photodetectors. In Figure 1a, a piece of CVD graphene with PMMA coated on one side is transferred on top of a WS_2-NDs/SiO_2 (500 nm)/Si sample. The entire sample assembly was then immersed in a diluted hydrofluoric acid (Figure 1b) during which the PMMA/graphene/WS_2-NDs can be released from the Si substrate after the SiO_2 is dissolved (Figure 1c). This transferrable PMMA/graphene/WS_2-ND nanohybrid can then be transferred on different functional substrates for device applications. In this work, the PMMA/graphene/WS_2-NDs were transferred on to a SiO_2/Si substrate with prefabricated Au/Ti electrodes and a AgNP-metafilm in the channel between the electrodes (Figure 1d). After the PMMA removal, the completed graphene/WS_2-NDs/AgNP-metafilm heterostructure nanohybrid photodetector is illustrated in Figure 1e. It should be mentioned that the method developed in this work for fabrication of the transferrable graphene/WS_2-ND samples is unique and advantageous in terms of preventing degradation of the LSPR effect of the AgNP-metafilm due to the exposure to sulfur vapor used for the WS_2-ND growth even with a SiO_2 overlayer. Figure S1a compares the optical absorption spectra of AgNP-metafilm before (solid) and after (dashed) the exposure to sulfur vapor at 450 °C for 1 h. A significantly reduced overall absorption, especially the disappearance of the LSPR peak due to the AgNP-metafilm, can be clearly seen in the latter, confirming the significant degradation of the LSPR by the AgNPs even with a 20 nm SiO_2 overlayer. The inset of Figure 1e depicts the zoomed-in view of the device structure with a WS_2-ND placed on the AgNP-metafilm. Upon light illumination, the photons absorbed by the WS_2-NDs will generate excitons (or photoexcited electron−hole pairs) that are separated at the graphene/WS_2-ND interface due to the interface built-in electric field.[31] A strong, localized light field around the WS_2-NDs by the LSPR effect of the AgNP-metafilm is illustrated by the green shading around the AgNP in the inset of Figure 1e. At a small distance of ∼20 nm between AgNPs and WS_2-NDs defined by the thickness of the SiO_2 spacer, the LSPR effect of

https://dx.doi.org/10.1021/acsanm.0c01360
ACS Appl. Nano Mater. 2020, 3, 7858−7868

the plasmonic AgNP-metafilm can lead to a significantly enhanced electromagnetic field, the so-called evanescent field, around the WS_2-NDs, and hence enhanced light absorption by the WS_2-NDs for improved photoresponsivity as we shall show in this work. The SiO_2 spacer also serves as a dielectric barrier layer to prevent electrical shorts between the graphene/WS_2-ND photodetector and the AgNP-metafilm. Generally, the evanescent field decays rapidly with distance from the surface of metallic plasmonic nanostructures over a range of a few to hundreds of nanometers depending on the specific nanostructure and the medium (SiO_2 in our case) around the nanostructure.[32,33] Therefore, the LSPR enhancement by the AgNP-metafilm is indeed affected by the thickness of the SiO_2. The thickness of SiO_2 should be thin enough for the enhanced plasmonic EM wave propagation in *z*-direction from the AgNPs to reach WS_2-NDs. On the other hand, the thickness of the SiO_2 layer must be thick enough to block the electrical leakage between the AgNPs and the graphene/WS_2-ND photodetector. In this study, we have found that a 20 nm thick SiO_2 can effectively block the current leakage between the graphene/WS_2-NDs and AgNP-metafilm while still allow much enhanced plasmonic EM field on the graphene/WS_2-NDs. It should be pointed out that the integrity of the AgNP-metafilm is the key to its generation of the LSPR evanescent field. If the AgNP-metafilm is contaminated by the sulfur vapor exposure during the WS_2-ND growth in samples with the WS_2-NDs directly fabricated on the AgNP-metafilms, the LSPR evanescent field seems negligible since the enhancement in the photoresponse of such devices is negligible as compared to the counterpart devices without the AgNP-metafilms (Figure S1b).

Figure 2a shows an optical image of a representative WS_2-ND sample fabricated on a SiO_2/Si substrate and the uniform distribution of the WS_2-NDs on the entire sample can be clearly seen. The Raman spectrum taken on this sample shows two distinctive peaks at 360.5 and 424.8 cm^{-1} (Figure S2), both can be indexed to WS_2, corresponding to the in-plane optical mode ($E_{2g}{}^1$) and the out-of-plane vibration mode (A_{1g}) of the sulfur atoms.[34,35] The Raman intensity map of the WS_2 $E_{2g}{}^1$ mode is displayed in Figure 2b, demonstrating the morphology and lateral dimensions of the WS_2-NDs, with sizes on the order of a few hundred nm. Figure 2c shows the AFM height profile measured along the green line in the AFM image (shown in the inset). Quantitatively, the lateral dimension of the WS_2-NDs is in the range of 200−300 nm that is consistent with the range revealed in the Raman map in Figure 2b. The height of the WS_2-NDs is in the range of 4−8 nm. Considering the approximately circular shape, large lateral dimension, and small vertical dimension of the WS_2 nanostructures revealed in Figure 2b,c, WS_2 nanodisks or WS_2-NDs are used to regard the WS_2 nanostructures in this work. An additional optical image of the graphene/WS_2-NDs after the graphene was transferred on the WS_2-NDs on the SiO_2/Si substrate is shown in Figure S3a. The inset depicts an optical image of the finished photodetector of the graphene/WS_2-ND/AgNP-metafilm with two Au electrodes. Figure S3b,c compares the Raman maps of the WS_2-NDs ($E_{2g}{}^1$ mode) and graphene (2D mode) on a graphene/WS_2-NDs sample, illustrating the uniform distribution of the WS_2-NDs on graphene. The weaker graphene 2D mode above the WS_2-NDs may be attributed to the interfacial interaction of graphene with WS_2-NDs. The Raman spectra of graphene on SiO_2/Si (black) and on the AgNP-metafilm/SiO_2/Si (green) substrates are illustrated in Figure 2d. In the former, the two graphene signature peaks at ∼1614.11 and 2719.19 cm^{-1} are assigned to the G and 2D bands, respectively. The G peak corresponds to the E_{2g} phonon at the Brillouin zone center and the 2D peak is the second order of the D band that corresponds to the A_{1g} breathing mode.[36−38] The absence of the graphene D peak (associated with defects) confirms the high quality of the CVD graphene in this work. The Raman spectrum of graphene on the AgNP-metafilm shows an overall enhancement in the intensity that can be attributed to the LSPR effect by the plasmonic nanostructures such as the AgNP-metafilm in this specific case. Comparing the two spectra shown in Figure 2d, the G and 2D Raman peaks of graphene with AgNPs are enhanced by 16 and 3 times, respectively. This plasmonic enhancement is consistent with that reported previously.[17,39−42] It should be noted that the Raman enhancement factors of the graphene peaks depend on the frequencies of the vibrational modes.[43] Therefore, the enhancement factors of the graphene G and 2D peaks are anticipated to be different.[17] In addition, the intense plasmonic EM field of the AgNPs could cause the lattice deformation of graphene and consequently enhance the D peak of graphene at 1387.26 cm^{-1}.[44] Both G and 2D peaks of graphene on the AgNP-metafilm are slightly red-shifted by ∼22 cm^{-1}. This red shift may be attributed to tensile strain after graphene is transferred on to the AgNP-metafilm. Representative AFM images of the SiO_2 (20 nm)/AgNP-metafilm sample at 10 and 1.0 μm^2 scan sizes are presented in Figure 2e,f. They show the expected nanoparticles along with a small number of defects. The topographical images of all regions of the sample showed consistently sized nanoparticles. The average roughness for the 10 × 10 μm^2 scans for all three areas was 12 ± 3 nm. A roughness of 11 ± 1 nm was measured for the 1.0 × 1.0 μm^2 scans. The topography and roughness of the sample without the SiO_2 coating were not significantly different than that for the SiO_2 (20 nm)/AgNP-metafilm sample. An SEM image taken on a representative AgNPs/SiO_2/Si sample is displayed in Figure 2g. The AgNPs exhibit irregular shapes. The average lateral dimension of the AgNPs is ranging from 20 to 120 nm with a mean diameter of 68 ± 27 nm and the size distribution is shown in the histogram (Figure S4). The absorption spectra for the AgNP-metafilm (blue), graphene/WS_2-NDs (green), and graphene/WS_2-ND/AgNP-metafilm (purple) are illustrated in Figure 2h. The maximum absorbance (the LSPR peak) for the AgNP-metafilm is at the wavelength of 442 nm, which is consistent with that reported previously.[30] The absorption spectrum of the graphene/WS_2-NDs shows broadband absorption from 400 to 700 nm with a small hump at ∼640 nm (band gap ∼1.94 eV for WS_2), which is consistent with previous reports.[10,45,46] On the absorption spectrum for the graphene/WS_2-ND/AgNP-metafilm sample, the AgNP's LSPR peak intensity is reduced and slightly red-shifted (∼19 nm), which could be ascribed to the damping in graphene as a semimetal as reported previously.[17,30] Interestingly, an enhanced absorption in a broadband of 400−700 nm can be observed on the graphene/WS_2-ND/AgNP-metafilm sample, which can be attributed to the enhanced absorption by the WS_2-NDs with the assistance of the LSPR evanescent field enabled by the AgNP-metafilm. The high AgNP density may cause a red shift for the plasmonic peak due to an interparticle coupling.[47] On the other hand, multiple layers of AgNPs may not increase the evanescent EM field at the graphene/WS_2-ND photodetectors considering the increased distance between the lower AgNP layers and the graphene/WS_2-ND photodetectors.

https://dx.doi.org/10.1021/acsanm.0c01360
ACS Appl. Nano Mater. 2020, 3, 7858−7868

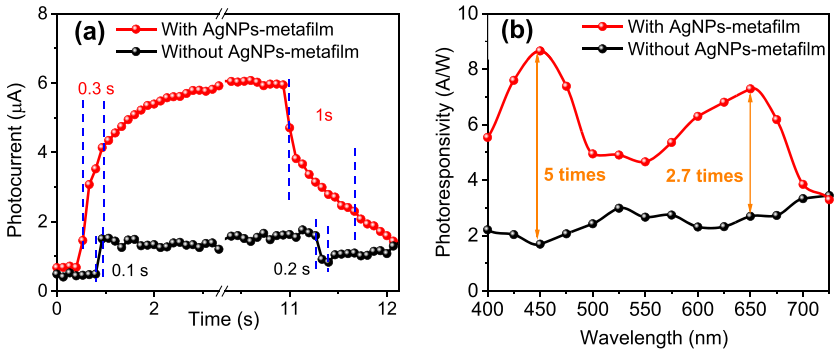

Figure 3. (a) Photocurrent response of the photodetectors with (red) and without (black) the AgNP-metafilm at 450 nm and light intensity of 0.15 mW/cm^2 under 0.8 V bias. (b) Photoresponsivity as a function of wavelength for the graphene/WS_2-ND photodetectors with (red) and without (black) the AgNP-metafilm. The source−drain bias voltage was 0.8 V for both devices.

Nevertheless, increasing the layers and density of the AgNPs may be an interesting topic for future research.

Figure 3a compares the photocurrents measured on the graphene/WS_2-ND photodetectors with (red) and without (black) the AgNP-metafilm under the illumination of 450 nm wavelength selected to be near the LSPR frequency of the AgNP-metafilm. The light intensity was 0.15 mW/cm^2 and the source−drain bias was 0.8 V. Remarkably, the photocurrent is enhanced by about five times in the graphene/WS_2-NDs with the AgNP-metafilm as compared to its counterpart without the AgNP-metafilm, which can be ascribed to the LSPR effect of the AgNP-metafilm. The response times of the photodetector are defined as rise time (t_{rise}) and fall time (t_{fall}), which correspond to the periods for the photocurrent to increase from 10 to 90% (or decrease from 90 to 10%) of its maximum value, respectively.[10,48] The t_{rise} and t_{fall} are 0.3 and 1.0 s for the graphene/WS_2-ND photodetector with the AgNP-metafilm, while shorter t_{rise} and t_{fall} of 0.1 and 0.2 s were observed on its counterpart without the AgNP-metafilm. The longer t_{rise} ∼ 0.3 s and t_{fall} ∼ 1.0 s together with the asymmetry of the dynamic response in the graphene/WS_2-ND/AgNP-metafilm photodetector could be attributed to unfavorable residual contamination at the graphene/WS_2-ND interface left during the graphene transfer on the WS_2-NDs and the second transfer of the graphene/WS_2-NDs on the AgNP-metafilm. While further investigation is necessary, this argument is consistent with the trend that shorter response times can be obtained on the similar samples with cleaner interfaces.[6,10,12] For example, in the graphene/WS_2-ND vdW heterostructure photodetectors with the WS_2-NDs directly grown on graphene, t_{rise} ∼ 10 ms and t_{fall} ∼ 20 ms were obtained.[10] On the graphene/WS_2-ND photodetectors with graphene transferred on WS_2-NDs, longer response times of t_{rise} ∼ 100 ms and t_{fall} ∼ 200 ms (black curve in Figure 3a) are about an order of magnitude larger. Since AgNPs degrade under the growth condition for WS_2-NDs, an additional transfer of the graphene/WS_2-NDs by dissolving the SiO_2 layer on the SiO_2/Si substrate was employed in this work to transfer the graphene/WS_2-ND assembly on the AgNP-metafilm. This additional transfer can certainly introduce more residues of chemicals to the graphene/WS_2-ND nanohybrid interface, which is most likely responsible for the further increased response times to t_{rise} ∼ 300 ms and t_{fall} ∼ 1000 ms as well as the asymmetry of the dynamic response due to the charge trapping at the interface (red curve in Figure 3a). This result therefore indicates that further research to improve the graphene/WS_2-ND interface is important and could lead to higher device performance. Figure S5 illustrates dynamic responses of the photocurrent of the graphene/WS_2-ND/AgNP-metafilm photodetector at three illumination wavelengths of 650, 550, and 450 nm. It is noticed that the amplitude of the photocurrent is the highest at the 450 nm illumination, which is anticipated from the peak at ∼450 nm in the spectral photoresponsivity shown in Figure 3b with the AgNP-metafilm due to the plasmonic light trapping by the AgNP-metafilm. In addition, the higher photocurrent amplitude at 650 nm, as compared to that at 550 nm, can also be attributed to the broad plasmonic peak at ∼650 nm in Figure 3b. At these three wavelengths, the t_{rise} and t_{fall} are comparable in the range of 0.3−1 s, respectively.

The photoresponsivity (R) is defined as $R = \frac{I_{ph}}{P_{in}}$, where I_{ph} is the photocurrent ($I_{ph} = I_{light} - I_{dark}$) and P_{in} is the illumination power. In Figure 3b, the spectral photoresponsivity of the two devices is compared in the visible wavelength range from 400 to 750 nm. For the graphene/WS_2-ND/AgNP-metafilm photodetector (red), the overall photoresponsivity in this spectrum range exhibits an obvious enhancement as compared to that of the counterpart device without the AgNP-metafilm (black). The enhanced photoresponsivity in the graphene/WS_2-ND/AgNP-metafilm photodetector can be attributed to the strong LSPR effect that originates from the AgNP-metafilm. There are two peaks in the spectral responsivity of this sample. The higher peak observed in the wavelength range of ∼400−475 nm around the LSPR wavelength (∼442 nm) of the AgNP-metafilm can be directly ascribed to the LSPR effect of the AgNP-metafilm on the absorption enhancement of the WS_2-NDs. This leads to the highest enhancement factor of ∼5 times, as shown in Figure 3b. This enhancement is anticipated from the LSPR effect of the AgNP-metafilm and confirms that the LSPR evanescent field generated by the AgNP-metafilm is indeed coupled effectively to the graphene/WS_2-NDs in the close proximity. In addition, a second peak of the responsivity at around 650 nm also exhibits a considerable enhancement of ∼2.7 times. This could be attributed to the large lateral size distribution of the AgNPs to allow the LSPR benefit to be extended to longer wavelengths (see more details in the FDTD simulation below) and the higher external quantum efficiency nearer the band gap of the WS_2-NDs. It should be realized that the band gap E_g for the few-layer WS_2 is 1.94 eV, which typically is observed as a shoulder in the absorption spectrum in the range of 640−700 nm (see Figure 2h). At longer wavelengths beyond the band gap cutoff of the WS_2-NDs, their

https://dx.doi.org/10.1021/acsanm.0c01360
ACS Appl. Nano Mater. 2020, 3, 7858−7868

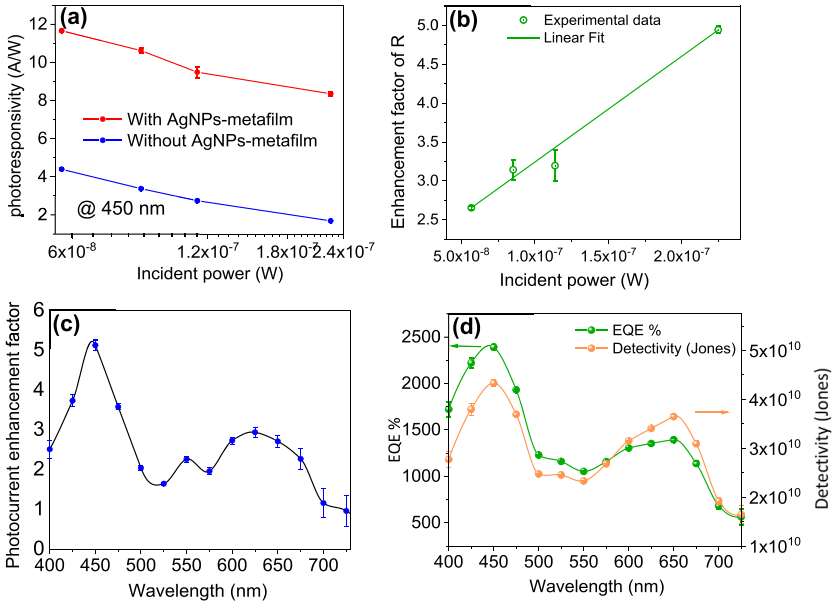

Figure 4. (a) Photoresponsivity of the graphene/WS_2-ND photodetectors with (red) and without (blue) the AgNP-metafilm at different incident power of the 450 nm illumination. The source−drain bias was 0.8 V. (b) Photoresponsivity enhancement as a function of incident power. (c) Photocurrent enhancement as a function of wavelength. (d) Measured external quantum efficiency (EQE) and detectivity D^* as a function of the wavelength under V_{sd} = 0.8 V.

light absorption decreases significantly, which seems consistent with the significantly reduced response at longer wavelengths beyond the cutoff at around 640−700 nm. Therefore, our results have demonstrated that the AgNP-metafilm can significantly enhance light absorption and hence broadband photoresponse over wavelengths from 400 to 700 nm through generation of a strong LSPR evanescent field using the AgNP-metafilm around the WS_2-NDs. Note that the SEM in Figure 2g shows a wide distribution of lateral dimensions (20−120 nm) and shapes of the AgNPs. In the simulation, the AgNPs were treated as semispheres with diameters in the range of 20−120 nm or radius in the range of 10−60 nm to illustrate their broadband LSPR effect.

Figure 4a depicts photoresponsivity as a function of the 450 nm illumination power. The highest photoresponsivities are 11.7 and 3.5 A/W, respectively, at the lowest incident power of 5.5×10^{-8} W for the graphene/WS_2-ND/AgNP-metafilm and graphene/WS_2-ND photodetectors. The photoresponsivity of both devices decreases monotonically with increasing illumination power, due to the higher quantum efficiencies from lower e−h pair recombination at lower illumination powers. However, the graphene/WS_2-ND/AgNP-metafilm device exhibits overall higher responsivity in this illumination power range than its counterpart without the AgNP-metafilm. This can be seen clearly from the enhancement factors, defined as the ratio of the photoresponsivities of the graphene/WS_2-ND photodetectors with and without the AgNP-metafilm (Figure 4b). The spectral photocurrent enhancement factor of the two devices, which is derived from the ratio between the black and red curves in Figure 3b, is displayed in Figure 4c. Quantitatively, the enhancement factor varies between the maximum value of 5 at around 450 nm near the LSPR peak of the AgNP-metafilm (442 nm) and the minimum value of 1.6 (525 nm) at the valley between the two peaks in Figure 3b. The smaller peak of the enhancement factor at around 650 nm may be explained by the fast fall of light absorption at longer wavelengths beyond the cutoff of WS_2 (on the right side of the peak) and the increasing quantum efficiency as the incident illumination wavelength is approaching the cutoff (from the left side of the peak).

The external quantum efficiency (EQE) and detectivity as a function of wavelength of the graphene/WS_2-ND/AgNP-metafilm nanohybrid photodetectors are plotted in Figure 4d. The EQE is defined as EQE = $(I_{ph}/e)/(P_{in}/h\nu)$, where h is the Planck constant, ν is the frequency of incident light, and e is the electron charge. The detectivity (D^*) can be defined as $D^* = \frac{A^{1/2}}{\mathrm{NEP}} = RA^{1/2}/i_n^{2^{1/2}}$ where A is the active area of the photodetector, NEP is the noise equivalent power, and i_n^2 is the noise current. With the assumption that the noise limiting the detectivity is dominated by shot noise from the dark current I_{dark} in the graphene channel, the detectivity can be expressed as $D^* = R\left[\left(\frac{A}{2eI_{dark}}\right)\right]^{1/2}$.[49] The maximum EQEs and D^* of 2390% and 4.3×10^{10} Jones are found at the wavelength of 450 nm. In Figure S6a, the photoresponsivity of the graphene/WS_2-ND/AgNP-metafilm photodetector was measured under different incident power (5.5×10^{-8}, 8.5×10^{-8}, and 1.2×10^{-7} W) and different bias voltages (0.4, 0.6, and 0.8 V) with 450 nm illumination. The measured photoresponsivity increases monotonically with the bias voltage at all different illumination powers and decreases with increasing the illumination power. The spectral photoresponsivities measured on transferred graphene/WS_2-NDs using the method developed in this work and on an in situ grown WS_2-NDs/graphene (no transfer) as we reported previously[10] are compared in Figure S6b. The two devices have comparable performance, indicating that the transferred graphene/WS_2-ND heterostructures were kept intact in the transfer process developed in this work.

To further study the impact of plasmonic effects, FDTD simulations were carried out on AgNPs. For simplicity, the AgNPs were treated as semispheres with diameters in the range

https://dx.doi.org/10.1021/acsanm.0c01360
ACS Appl. Nano Mater. 2020, 3, 7858−7868

of 20−120 nm or radius in the range of 10−60 nm considering the wide distribution of lateral dimension (20−120 nm) and shapes of AgNPs revealed in SEM analysis in Figures 2g and S4. To see how such a feature plays a key role in the enhancement of photoresponsitivity reported in Figure 3b, we used FDTD simulation (Lumerical) to study the plasmonic mode profiles and absorption cross sections of AgNPs with different lateral sizes. The system considered in this paper is schematically shown in Figure 5a based on the device structure

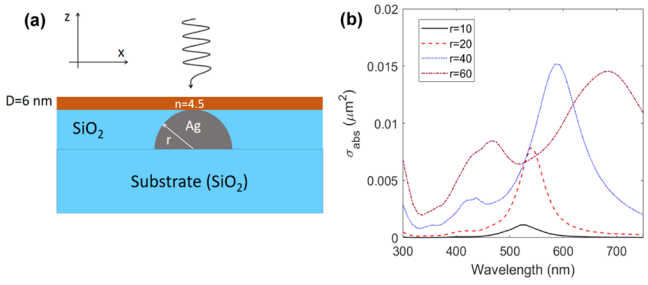

Figure 5. (a) Diagram of the structure adopted for FDTD simulations of the plasmonic response of the AgNP. The AgNP (semisphere) has the radius of r and embedded in SiO_2. The thin layer on the top with thickness of D = 6 nm represents the WS_2-ND and graphene. (b) Absorption cross section of the structure shown in (a) for different radius values of 10, 20, 40, and 60 nm of the AgNP (legends in nm).

shown in Figure 1e. The structure includes a semispherical AgNP with radius r on a glass substrate. The AgNPs are considered to be embedded in a silica layer, and on the top, there is a thin layer with a thickness (D) of 6 nm. This layer has an effective refractive index of 4.5 and effectively represents the top WS_2-NDs and graphene. It should be realized that the dimension of the WS_2-NDs may correlate to their optical properties and affect the graphene/WS_2-ND photodetector's spectral range and responsivity. A future research on such an effect of the WS_2-ND dimension will be interesting to both understanding the underlying physics and facilitating the practical applications of the WS_2-NDs.

The results of the calculations for the absorption cross section are shown in Figure 5b. For small r, e.g., r = 10 nm (solid line), the absorption contains a single peak at about 520 nm. As the size of the AgNP increases, this peak is red-shifted as another peak is formed at a shorter wavelength. For r = 60 nm (dashed-dotted line), the spectrum includes two peaks with a main broad peak at 685 nm and another peak at 465 nm. Therefore, the spectrum seen in Figure 2h (graphene/WS_2-ND/AgNP-metafilm) is the result of a weighted average of the spectra seen in Figure 5b, considering the size distribution of the AgNPs (Figure 2g). Considering the results shown in Figure 5b, we believe that the photoresponsivity presented in Figure 3b is the result of plasmonic enhancement of optical excitation at two major wavelength ranges.[50−53] The first happens around the band gap of WS_2-NDs and can be involved with the interband excitons. The second occurs at the upper band edge (or excited states above the band gap) of the WS_2-NDs, close to the overall major plasmonic peak of the AgNP-metafilm seen in Figure 2h (or that of graphene/WS_2-ND/AgNP-metafilm), i.e., at 450 nm. In this wavelength range, one expects that the plasmon field enhancement promotes excitation of the electron/hole pairs.[52,53] Considering the wide ranges of AgNP sizes (20−120 nm) as shown in Figures 2g and S4, the contributions of the stronger peaks beyond 520 nm in Figure 5b are most probably suppressed to some extent by the relatively smaller number of AgNPs with larger sizes. Despite this, since such peaks are quite broad, their presence can explain the broad spectrum of graphene/WS_2-ND/AgNP-metafilm in Figure 2h (purple line), particularly the feature on its longer wavelength side. On the other hand, such a peak can be associated with the combined contribution of the main peaks around 520 and the secondary peaks of the larger AgNPs around 450 nm seen in Figure 6b. This may explain the slope of the shorter wavelength side of the peak seen in Figure 2h (purple line). Of course, in terms of the overall wavelength, there are some discrepancies between the simulation results and those presented in Figure 2h. A main reason for this is the fact that we approximated the shapes of the AgNPs as semispheres.

To see this better, in Figure 6 we show the mode profiles of the structure for r = 60 and 10 nm. Here, a and b refer to the profiles for r = 60 nm and at 685 and 465 nm, respectively. Figure 6c shows the mode profile for r = 10 nm at 520 nm. Note that in all of these cases we consider the incident beam is polarized along the x axis (Figure 5a). The results represented in Figure 6 offer two main observations. The first is the fact that the upper thin layer (D = 6 nm), which represents the WS_2-NDs and graphene, pulls the plasmonic modes of the AgNP-metafilm upward. The second observation is the penetration of the plasmonic field into this layer. The combination of these two suggests that the AgNP-metafilm with 60 nm radius can support the plasmonic enhancement of the optical excitations of the WS_2-NDs at 685 nm,[50] which contributes to the photoresponsivity rise at 650 nm. Additionally, the plasmon modes of such AgNPs at 465 nm can also support formation of the peak of the photoresponsivity seen at 450 nm (Figure 3b). The photoresponsivity peak at 450 nm is also promoted by the AgNP-metafilm with smaller sizes. In fact, as shown in Figure 6c, for r = 10 nm, the plasmon mode penetration into the WS_2-NDs is expected to be significant.

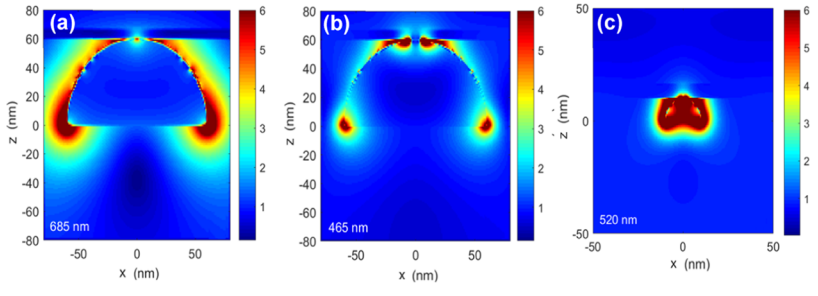

Figure 6. FDTD simulated electromagnetic field mode profiles of a AgNP with r = 60 nm (a, b) and 10 nm (c).

https://dx.doi.org/10.1021/acsanm.0c01360
ACS Appl. Nano Mater. 2020, 3, 7858−7868

The plasmon coupling between the Ag nanoparticles is expected to be insignificant. This is because of the fact that the range of the plasmon field of the nanoparticles in the plane of the film is far less than the interparticle spacing.

4. CONCLUSIONS

In summary, a graphene/WS_2-ND/AgNP-metafilm vdW heterostructure nanohybrid has been developed in this work to enable a strong exciton−plasmon coupling. This nanohybrid integrates a nonmetallic plasmonic WS_2-ND/graphene vdW heterostructure with a metallic plasmonic AgNP-metafilm for superposition of the plasmonic-enhanced absorption of visible light. A critical step in this integration is the development of a process for fabrication of the transferrable graphene/WS_2-ND nanohybrids that can be transferred on to the AgNP-metafilm. This can prevent degradation of the LSPR effect of the AgNP-metafilm from the contamination by the sulfur vapor required for the growth of the WS_2-NDs. In the obtained graphene/WS_2-ND/AgNP-metafilm heterostructures, the controlled spacing of ∼20 nm between graphene/WS_2-NDs and the AgNP-metafilm by the SiO_2 overlayer on the AgNPs allows effective coupling of excitons generated upon light illumination in the WS_2-NDs and the plasmonic evanescent EM field in the vicinity of the AgNP-metafilm, resulting in a significantly enhanced photoresponsivity. Under the light illumination of 450 nm of an incident power of 5.5×10^{-8} W, high photoresponsivity of 11.7 A/W, EQE of 2390%, and detectivity D^* of 4.3×10^{10} Jones have been obtained at a bias voltage of 0.8 V, which represent a significant improvement over that of the counterpart devices without the plasmonic AgNP-metafilm. For example, the responsivity of the former is more than five times of that on the latter, confirming that a significantly enhanced light absorption can be achieved by integrating the graphene/WS_2-NDs and AgNP-metafilm in the graphene/WS_2-ND/AgNP-metafilm heterostructure nanohybrids. Considering that both WS_2-NDs (or in general TMDC-NDs)/graphene and AgNP-metafilm can be obtained using chemical or physical vapor deposition in wafer size as illustrated in this work, the developed approach is promising for the practical photodetectors and other optoelectronic applications.

■ ASSOCIATED CONTENT

Supporting Information

The Supporting Information is available free of charge at https://pubs.acs.org/doi/10.1021/acsanm.0c01360.

(Figure S1) (a) UV−vis absorption spectra of the AgNP-metafilm before (solid line) and after (dashed line) exposure to the sulfur vapor at 450 °C for 1 h; (b) photoresponse of the WS_2-ND/graphene photodetectors without a AgNP-metafilm (black) and with a AgNP-metafilm (blue) that was exposed to the sulfur vapor at 450 °C for 1 h before the photoresponse measurement at 5 V; (Figure S2) Raman spectrum of a representative graphene/WS_2-ND sample after transfer in the low-wave number range; (Figure S3) (a) Optical image of graphene transferred on WS_2-NDs on the SiO_2/Si substrate and inset: optical image of the photodetector of the graphene/WS_2-ND/AgNP-metafilm with two Au electrodes, Raman maps of (b) WS_2-NDs (E_{2g}^1 mode) and (c) graphene (2D mode) on the WS_2-NDs; (Figure S4) histogram of the lateral dimension distribution of the AgNPs grown on the SiO_2/Si substrates based on the SEM image of the sample; (Figure S5) dynamic photocurrent in response to light on/off with three incident light wavelengths of 650 nm (red), 550 nm (green), and 450 nm (blue); (Figure S6) (a) Photoresponsivity of the graphene/WS_2-ND/AgNP-metafilm nanohybrid photodetectors at different incident light powers and different bias voltages across the devices. The wavelength of the incident light was fixed at λ = 450 nm, (b) comparison of the photoresponsivity of the WS_2-ND/graphene photodetectors: before (black) and after (red) transfer measured under the same condition at 0.8 V (PDF)

■ AUTHOR INFORMATION

Corresponding Authors

Mohammed Alamri − *Department of Physics and Astronomy, University of Kansas, Lawrence, Kansas 66045, United States; Department of Physics, University of Umm Al-Qura, Makkah 21955, Saudi Arabia;* orcid.org/0000-0002-7473-8644; Email: mohammed.alamri@ku.edu

Judy Wu − *Department of Physics and Astronomy, University of Kansas, Lawrence, Kansas 66045, United States*; Email: jwu@ku.edu

Authors

Bo Liu − *Department of Physics and Astronomy, University of Kansas, Lawrence, Kansas 66045, United States;* orcid.org/0000-0003-0298-8238

Seyed M. Sadeghi − *Department of Physics and Astronomy, The University of Alabama in Huntsville, Alabama 35899, United States*

Dan Ewing − *Department of Energy's National Security Campus, Kansas City, Missouri 64147, United States*

Amy Wilson − *Department of Energy's National Security Campus, Kansas City, Missouri 64147, United States*

Jennifer L. Doolin − *Department of Chemistry, University of Kansas, Lawrence, Kansas 66045, United States*

Cindy L. Berrie − *Department of Chemistry, University of Kansas, Lawrence, Kansas 66045, United States;* orcid.org/0000-0003-2422-8141

Complete contact information is available at: https://pubs.acs.org/10.1021/acsanm.0c01360

Author Contributions

M.A. and J.W. designed the experiment. M.A. performed the sample characterization. B.L. participated in the sample preparation. S.M.S. did the simulation. J.L.D. and C.L.B. carried out the sample characterization. M.A. and J.W. led the effort in manuscript writing. All authors contributed to the discussions of the results and development of the manuscript.

Notes

The authors declare no competing financial interest.

■ ACKNOWLEDGMENTS

This research was supported by Plant Directed Research and Development funds from the Department of Energy's Kansas City National Security Campus, operated and managed by Honeywell Federal Manufacturing and Technologies, LLC under contract No. DE-NA0002839. The authors acknowledge support in part by ARO contract No. ARO-W911NF-16-1-0029 and NSF contract Nos. NSF-DMR-1909292, NSF-

ECCS-1809293, and NSF-DMR-1508494. M.A. acknowledges the support from Umm Al-Qura University.

REFERENCES

(1) Bolotin, K. I.; Sikes, K. J.; Jiang, Z.; Klima, M.; Fudenberg, G.; Hone, J.; Kim, P.; Stormer, H. Ultrahigh electron mobility in suspended graphene. *Solid State Commun.* **2008**, *146*, 351−355.

(2) Nair, R. R.; Blake, P.; Grigorenko, A. N.; Novoselov, K. S.; Booth, T. J.; Stauber, T.; Peres, N. M.; Geim, A. K. Fine structure constant defines visual transparency of graphene. *Science* **2008**, *320*, 1308.

(3) Liu, X.; Hu, J.; Yue, C.; Della Fera, N.; Ling, Y.; Mao, Z.; Wei, J. High performance field-effect transistor based on multilayer tungsten disulfide. *ACS Nano* **2014**, *8*, 10396−10402.

(4) Huang, H.; Wang, J.; Hu, W.; Liao, L.; Wang, P.; Wang, X.; Gong, F.; Chen, Y.; Wu, G.; Luo, W. Highly sensitive visible to infrared MoTe2 photodetectors enhanced by the photogating effect. *Nanotechnology* **2016**, *27*, No. 445201.

(5) Konstantatos, G.; Badioli, M.; Gaudreau, L.; Osmond, J.; Bernechea, M.; De Arquer, F. P. G.; Gatti, F.; Koppens, F. H. Hybrid graphene−quantum dot phototransistors with ultrahigh gain. *Nat. Nanotechnol.* **2012**, *7*, 363−368.

(6) Gong, M.; Liu, Q.; Cook, B.; Kattel, B.; Wang, T.; Chan, W.-L.; Ewing, D.; Casper, M.; Stramel, A.; Wu, J. Z. All-printable ZnO quantum dots/graphene van der Waals heterostructures for ultrasensitive detection of ultraviolet light. *ACS Nano* **2017**, *11*, 4114−4123.

(7) Kuiri, M.; Chakraborty, B.; Paul, A.; Das, S.; Sood, A.; Das, A. Enhancing photoresponsivity using MoTe2-graphene vertical heterostructures. *Appl. Phys. Lett.* **2016**, *108*, No. 063506.

(8) Shao, D.; Gao, J.; Chow, P.; Sun, H.; Xin, G.; Sharma, P.; Lian, J.; Koratkar, N. A.; Sawyer, S. Organic−inorganic heterointerfaces for ultrasensitive detection of ultraviolet light. *Nano Lett.* **2015**, *15*, 3787−3792.

(9) Gong, Y.; Liu, Q.; Wilt, J. S.; Gong, M.; Ren, S.; Wu, J. Wrapping cytochrome c around single-wall carbon nanotube: engineered nanohybrid building blocks for infrared detection at high quantum efficiency. *Sci. Rep.* **2015**, *5*, No. 11328.

(10) Alamri, M.; Gong, M.; Cook, B.; Goul, R.; Wu, J. Z. Plasmonic WS2 Nanodiscs/Graphene van der Waals Heterostructure Photodetectors. *ACS Appl. Mater. Interfaces* **2019**, *11*, 33390−33398.

(11) Liu, Q.; Cook, B.; Gong, M.; Gong, Y.; Ewing, D.; Casper, M.; Stramel, A.; Wu, J. Printable transfer-free and wafer-size MoS2/Graphene van der Waals heterostructures for high-performance photodetection. *ACS Appl. Mater. Interfaces* **2017**, *9*, 12728−12733.

(12) Lu, R.; Liu, J.; Luo, H.; Chikan, V.; Wu, J. Z. Graphene/GaSe-nanosheet hybrid: towards high gain and fast photoresponse. *Sci. Rep.* **2016**, *6*, No. 19161.

(13) He, J.; Fan, C.; Wang, J.; Cheng, Y.; Ding, P.; Liang, E. Plasmonic Nanostructure for Enhanced Light Absorption in Ultrathin Silicon Solar Cells. *Adv. OptoElectron.* **2012**, *2012*, No. 592754.

(14) Schaadt, D.; Feng, B.; Yu, E. Enhanced semiconductor optical absorption via surface plasmon excitation in metal nanoparticles. *Appl. Phys. Lett.* **2005**, *86*, No. 063106.

(15) Miao, J.; Hu, W.; Jing, Y.; Luo, W.; Liao, L.; Pan, A.; Wu, S.; Cheng, J.; Chen, X.; Lu, W. Surface plasmon-enhanced photodetection in few layer MoS2 phototransistors with Au nanostructure arrays. *Small* **2015**, *11*, 2392−2398.

(16) Liu, Y.; Cheng, R.; Liao, L.; Zhou, H.; Bai, J.; Liu, G.; Liu, L.; Huang, Y.; Duan, X. Plasmon resonance enhanced multicolour photodetection by graphene. *Nat. Commun.* **2011**, *2*, No. 579.

(17) Lu, R.; Konzelmann, A.; Xu, F.; Gong, Y.; Liu, J.; Liu, Q.; Xin, M.; Hui, R.; Wu, J. Z. High sensitivity surface enhanced Raman spectroscopy of R6G on in situ fabricated Au nanoparticle/graphene plasmonic substrates. *Carbon* **2015**, *86*, 78−85.

(18) Goul, R.; Das, S.; Liu, Q.; Xin, M.; Lu, R.; Hui, R.; Wu, J. Z. Quantitative analysis of surface enhanced Raman spectroscopy of Rhodamine 6G using a composite graphene and plasmonic Au nanoparticle substrate. *Carbon* **2017**, *111*, 386−392.

(19) Chen, P.; Qiu, H.; Xu, S.; Liu, X.; Li, Z.; Hu, L.; Li, C.; Guo, J.; Jiang, S.; Huo, Y. A novel surface-enhanced Raman spectroscopy substrate based on a large area of MoS2 and Ag nanoparticles hybrid system. *Appl. Surf. Sci.* **2016**, *375*, 207−214.

(20) Alamri, M.; Sakidja, R.; Goul, R.; Ghopry, S.; Wu, J. Z. Plasmonic Au Nanoparticles on 2D MoS2/Graphene van der Waals Heterostructures for High-Sensitivity Surface-Enhanced Raman Spectroscopy. *ACS Appl. Nano Mater.* **2019**, *2*, 1412−1420.

(21) Luther, J. M.; Jain, P. K.; Ewers, T.; Alivisatos, A. P. Localized surface plasmon resonances arising from free carriers in doped quantum dots. *Nat. Mater.* **2011**, *10*, 361−366.

(22) Gong, M.; Ewing, D.; Casper, M.; Stramel, A.; Elliot, A.; Wu, J. Z. Controllable Synthesis of Monodispersed Fe1−x S2 Nanocrystals for High-Performance Optoelectronic Devices. *ACS Appl. Mater. Interfaces* **2019**, *11*, 19286−19293.

(23) Gong, M.; Sakidja, R.; Liu, Q.; Goul, R.; Ewing, D.; Casper, M.; Stramel, A.; Elliot, A.; Wu, J. Z. Broadband photodetectors enabled by localized surface plasmonic resonance in doped iron pyrite nanocrystals. *Adv. Opt. Mater.* **2018**, *6*, No. 1701241.

(24) Wu, J. *Exploration of Uncooled Quantum Infrared Detectors Based on Quantum Dots/Graphene Heterostructures.*; SPIE, 2020; Vol. *11407*.

(25) Ghopry, S. A.; Alamri, M. A.; Goul, R.; Sakidja, R.; Wu, J. Z. Extraordinary Sensitivity of Surface-Enhanced Raman Spectroscopy of Molecules on MoS2 (WS2) Nanodomes/Graphene van der Waals Heterostructure Substrates. *Adv. Opt. Mater.* **2019**, *7*, No. 1801249.

(26) Liu, B.; Gutha, R. R.; Kattel, B.; Alamri, M.; Gong, M.; Sadeghi, S. M.; Chan, W.-L.; Wu, J. Z. Using Silver Nanoparticles-Embedded Silica Metafilms as Substrates to Enhance the Performance of Perovskite Photodetectors. *ACS Appl. Mater. Interfaces* **2019**, *11*, 32301−32309.

(27) Liu, Q.; Gong, Y.; Wilt, J. S.; Sakidja, R.; Wu, J. Synchronous growth of AB-stacked bilayer graphene on Cu by simply controlling hydrogen pressure in CVD process. *Carbon* **2015**, *93*, 199−206.

(28) Liu, J.; Xu, G.; Rochford, C.; Lu, R.; Wu, J.; Edwards, C. M.; Berrie, C. L.; Chen, Z.; Maroni, V. A. Doped graphene nanohole arrays for flexible transparent conductors. *Appl. Phys. Lett.* **2011**, *99*, No. 023111.

(29) Xu, G. W.; Lu, R. T.; Liu, J. W.; Chiu, H. Y.; Hui, R. Q.; Wu, J. Z. Photodetection Based on Ionic Liquid Gated Plasmonic Ag Nanoparticle/Graphene Nanohybrid Field Effect Transistors. *Adv. Opt. Mater.* **2014**, *2*, 729−736.

(30) Xu, G.; Liu, J. W.; Wang, Q.; Hui, R. Q.; Chen, Z. J.; Maroni, V. A.; Wu, J. Plasmonic Graphene Transparent Conductors. *Adv. Mater.* **2012**, *24*, OP71−OP76.

(31) Zhang, W.; Chuu, C.-P.; Huang, J.-K.; Chen, C.-H.; Tsai, M.-L.; Chang, Y.-H.; Liang, C.-T.; Chen, Y.-Z.; Chueh, Y.-L.; He, J.-H. Ultrahigh-gain photodetectors based on atomically thin graphene-MoS 2 heterostructures. *Sci. Rep.* **2014**, *4*, No. 3826.

(32) Maier, S. A. *Plasmonics: Fundamentals and Applications*; Springer Science & Business Media, 2007.

(33) Willets, K. A.; Van Duyne, R. P. Localized surface plasmon resonance spectroscopy and sensing. *Annu. Rev. Phys. Chem.* **2007**, *58*, 267−297.

(34) Berkdemir, A.; Gutiérrez, H. R.; Botello-Méndez, A. R.; Perea-López, N.; Elías, A. L.; Chia, C.-I.; Wang, B.; Crespi, V. H.; López-Urías, F.; Charlier, J.-C.; Terrones, H.; Terrones, M. Identification of individual and few layers of WS 2 using Raman spectroscopy. *Sci. Rep.* **2013**, *3*, No. 1755.

(35) Qiao, S.; Yang, H.; Bai, Z.; Peng, G.; Zhang, X. In *Identifying the Number of WS2 Layers via Raman and Photoluminescence Spectrum*, 5th International Conference on Mechatronics, Materials, Chemistry and Computer Engineering (ICMMCCE 2017); Atlantis Press, 2017.

(36) Ferrari, A. C.; Meyer, J.; Scardaci, V.; Casiraghi, C.; Lazzeri, M.; Mauri, F.; Piscanec, S.; Jiang, D.; Novoselov, K.; Roth, S. Raman spectrum of graphene and graphene layers. *Phys. Rev. Lett.* **2006**, *97*, No. 187401.

(37) Ferrari, A. C.; Basko, D. M. Raman spectroscopy as a versatile tool for studying the properties of graphene. *Nat. Nanotechnol.* **2013**, *8*, 235.

https://dx.doi.org/10.1021/acsanm.0c01360
ACS Appl. Nano Mater. 2020, 3, 7858−7868

(38) Gupta, A.; Chen, G.; Joshi, P.; Tadigadapa, S.; Eklund, P. Raman scattering from high-frequency phonons in supported n-graphene layer films. *Nano Lett.* **2006**, *6*, 2667−2673.
(39) Paria, D.; Jeong, H.-H.; Vadakkumbatt, V.; Deshpande, P.; Fischer, P.; Ghosh, A.; Ghosh, A. Graphene−silver hybrid devices for sensitive photodetection in the ultraviolet. *Nanoscale* **2018**, *10*, 7685−7693.
(40) Heeg, S.; Fernandez-Garcia, R.; Oikonomou, A.; Schedin, F.; Narula, R.; Maier, S. A.; Vijayaraghavan, A.; Reich, S. Polarized plasmonic enhancement by Au nanostructures probed through Raman scattering of suspended graphene. *Nano Lett.* **2013**, *13*, 301−308.
(41) Maiti, R.; Haldar, S.; Majumdar, D.; Singha, A.; Ray, S. Hybrid opto-chemical doping in Ag nanoparticle-decorated monolayer graphene grown by chemical vapor deposition probed by Raman spectroscopy. *Nanotechnology* **2017**, *28*, No. 075707.
(42) Prakash, G.; Srivastava, R. K.; Gupta, S. N.; Sood, A. Plasmon-induced efficient hot carrier generation in graphene on gold ultrathin film with periodic array of holes: Ultrafast pump-probe spectroscopy. *J. Chem. Phys.* **2019**, *151*, No. 234712.
(43) Balasubramanian, K.; Zuccaro, L.; Kern, K. Tunable Enhancement of Raman Scattering in Graphene-Nanoparticle Hybrids. *Adv. Funct. Mater.* **2014**, *24*, 6348−6358.
(44) Ghamsari, B. G.; Olivieri, A.; Variola, F.; Berini, P. Enhanced Raman scattering in graphene by plasmonic resonant Stokes emission. *Nanophotonics* **2014**, *3*, 363−371.
(45) Zeng, L.; Tao, L.; Tang, C.; Zhou, B.; Long, H.; Chai, Y.; Lau, S. P.; Tsang, Y. H. High-responsivity UV−vis photodetector based on transferable WS 2 film deposited by magnetron sputtering. *Sci. Rep.* **2016**, *6*, No. 20343.
(46) Zhao, W.; Ghorannevis, Z.; Chu, L.; Toh, M.; Kloc, C.; Tan, P.-H.; Eda, G. Evolution of electronic structure in atomically thin sheets of WS2 and WSe2. *ACS Nano* **2013**, *7*, 791−797.
(47) Halas, N. J.; Lal, S.; Chang, W.-S.; Link, S.; Nordlander, P. Plasmons in strongly coupled metallic nanostructures. *Chem. Rev.* **2011**, *111*, 3913−3961.
(48) Goushcha, A. O.; Tabbert, B. On response time of semiconductor photodiodes. *Opt. Eng.* **2017**, *56*, No. 097101.
(49) Wu, J. Graphene. In *Transparent Conductive Materials*; Wiley, 2019; pp 165−192.
(50) Kern, J.; Trügler, A.; Niehues, I.; Ewering, J.; Schmidt, R.; Schneider, R.; Najmaei, S.; George, A.; Zhang, J.; Lou, J. Nanoantenna-enhanced light−matter interaction in atomically thin WS2. *ACS Photonics* **2015**, *2*, 1260−1265.
(51) Chen, H.; Yang, J.; Rusak, E.; Straubel, J.; Guo, R.; Myint, Y. W.; Pei, J.; Decker, M.; Staude, I.; Rockstuhl, C.; et al. Manipulation of photoluminescence of two-dimensional MoSe 2 by gold nano-antennas. *Sci. Rep.* **2016**, *6*, No. 22296.
(52) Sadeghi, S. M.; Wing, W. J.; Gutha, R. R.; Goul, R. W.; Wu, J. Z. Functional metal-oxide plasmonic metastructures: Ultrabright semiconductor quantum dots with polarized spontaneous emission and suppressed Auger recombination. *Phys. Rev. Appl.* **2019**, *11*, No. 024045.
(53) Wing, W. J.; Sadeghi, S. M.; Gutha, R. R.; Campbell, Q.; Mao, C. Metallic nanoparticle shape and size effects on aluminum oxide-induced enhancement of exciton-plasmon coupling and quantum dot emission. *J. Appl. Phys.* **2015**, *118*, No. 124302.

https://dx.doi.org/10.1021/acsanm.0c01360
ACS Appl. Nano Mater. 2020, 3, 7858−7868